DOI 10.1007/s11182-024-03156-7
Russian Physics Journal, Vol. 67, No. 5, May, 2024

PRINCIPLES OF INCREASING THE STRENGTH AND TOUGHNESS OF FERRITIC/MARTENSITIC STEEL PRODUCED BY COLD ROLLING

A. V. Ganeev, A. A. Frik, R. K. Islamgaliev, N. A. Khaybulina, and M. A. Nikitina UDC 621

This paper presents the results of studying the evolution of the structure and mechanical properties of 12Cr–2W *ferritic/martensitic steel after cold rolling and additional heat treatment. X-ray diffraction analysis, transmission electron microscopy, and electron backscattering diffraction were used to study the structure. A significant increase of tensile strength up to a tensile strength of 1380 MPa was observed after cold rolling to 50% reduction and subsequent re-quenching from the austenite region. Compared to samples subjected to standard treatment, the use of this combined treatment led to the increase of impact toughness by 22 times up to 550 kJ/m2. The principles of achieving enhanced strength and toughness by reducing the grain size and increasing the fraction of carbides and the share of coincident site lattice (CSL) boundaries are discussed.*

Keywords: ferritic/martensitic steels, strength, toughness, ductile–brittle transition temperature.

INTRODUCTION

Strength and toughness are important properties of steels to reduce weight and increase reliability. The strength of steels can be improved using various strengthening mechanisms, including grain refinement and dispersion hardening [1, 2]. For example, the microstructure of ferritic/martensitic steels processed by equal channel angular pressing or rolling has been investigated recently to estimate the impact of grain refinement on strength and ductility [2, 3].

At the same time, the toughness decreases after grain refinement in various metallic materials because of embrittlement due to decrease in ductility [4]. From the other side, the grain refinement significantly increased the amount of grain boundaries in the ultrafine-grained structure. When a cleavage crack propagates through several grains, both the emission of crack tip dislocations and the formation of cleavage facets are interrupted by the grain boundaries resulting in enhancement of toughness [5].

Since crack propagation at the impact tests is accompanied by dislocation motion, coincident site lattice (CSL) boundaries can provide an effective barrier to hinder dislocation gliding. Therefore, one can assume that materials containing numerous CSL boundaries can demonstrate simultaneously the improved strength and toughness. Recently, the formation of CSL boundaries after grain refinement and additional re-quenching has been observed in the 12Cr–2W ferritic/martensitic steel [2, 3]. In the present work, the 12Cr–2W ferritic/martensitic steel has been used to investigate the influence of various defects: grain boundaries, carbides, and CSL boundaries on strength and toughness.

Ufa University of Science and Technology, Ufa, Russia, e-mail: ganeev.av@ugatu.su; frikaleksandra@gmail.com; rinatis@mail.ru; nkhaibulinaw@yandex.ru; nkhaibulinaw@yandex.ru; nik.marina.al@gmail.com. Original article submitted December 27, 2023.

TABLE 1. Chemical Composition of the Steel in wt.%

Fe	C	Cr	W	Mo	Ni	V
84.824	0.138	10.88	1.806	0.458	1.687	0.207

EXPERIMENTAL

Chemical composition of the 12Cr–2W ferritic/martensitic steel is presented in Table 1. Standard heat treatment of steel is quenching from a temperature of 1050°C into oil and tempering at 550–800°C followed by cooling in air. Plates with dimensions of $28 \times 14.5 \times 85$ mm^3 were prepared from initial rod subjected to standard heat treatment. The plates were rolled on a laboratory rolling mill with a roll diameter of 70 mm and a rotation speed of 1.5 m/min with a reduction per pass of 6% to a final thickness of 4.3 mm. After total reduction of 30% and 50%, parts were cut off from the samples to study their structure, and the remaining part was subjected to subsequent rolling to 70% reduction. To further improve the mechanical properties, post-deformation heat treatment was applied at the temperature exceeding that of the ferrite/austenite phase transformation (at 850°C for one hour) followed by quenching in oil (re-quenching).

The microstructure was studied using a JEM-2100 transmission electron microscope with an accelerating voltage of 200 kV. The surface fracture was studied on a JSM-6390 scanning microscope with an accelerating voltage of 30 kV. To prepare foils, discs with a diameter of 3 mm were cut out from the samples. Next, these disks were mechanically thinned to a thickness of 0.11–0.15 mm. Using the Tenupol-5 installation, final thinning was carried out using electropolishing at a temperature of 20 ± 5°C and voltage of 20–50 V in a 10% perchloric acid $HClO_4$ electrolyte with butanol.

To calculate the lattice parameter, we used X-ray diffraction with a Rigaku Ultima IV diffractometer employing the Bragg–Brentano focusing method. To study the phase composition of carbides with small volume fraction, we used transmission X-ray diffraction [6] realized on a Rigaku Ultima IV diffractometer using CuKα radiation (40 kV and 40 mA). In this case, the diffraction patterns were obtained on foils with thickness of 5–7 μm using a parallel beam in the transmission regime. As a result, carbide peaks were identified using the PDXL software, and quantitative estimation of their volume fraction was performed by the Rietveld method [7].

Our tensile tests were carried out on an Instron 5982 universal testing system at a strain rate of 10^{-3} mm/s using specimens with gage dimensions of $0.5 \times 1 \times 5$ mm^3. The Charpy impact tests were conducted using full-size 2 mm V-notched specimens with dimensions of $7.5 \times 8 \times 55$ mm^3 on an Instron 9350 machine. The ductile-to-brittle transition temperature (DBTT) was determined from the Charpy curve as the temperature corresponding to the half value between the maximum and minimum of the impact toughness. To establish the DBTT, tests were carried out in the temperature range 60–120°C. The test specimens were cut along the rolling direction. The results obtained are presented in Tables 2–4 and are discussed below.

RESULTS

Standard heat treatment of the 12Cr–2W ferritic/martensitic steel is quenching from a temperature of 1050°C into oil and tempering at 550–800°C followed by cooling in air [8]. Figure 1 shows the microstructure of steel in the initial hot-rolled state with ferrite grains along the boundaries of which carbides are located. After holding at temperatures in the range 1040–1150°C, almost complete dissolution of carbides occurs, and with further rapid cooling in oil, martensite is formed. Subsequent tempering at temperatures of 750–800°C leads to the decomposition of martensite and precipitation of $M_{23}C_6$ carbides (50–170 nm in size) and MX carbonitrides (30–50 nm in size).

The non-uniform distribution of particles observed in the initial samples (Fig. 1*a*) usually reduces the deformability of the material due to the presence of local stresses. Therefore, before deformation, the initial samples were subjected to standard treatment by heating at 1050°C for 1 h with subsequent quenching and tempering at 800°C

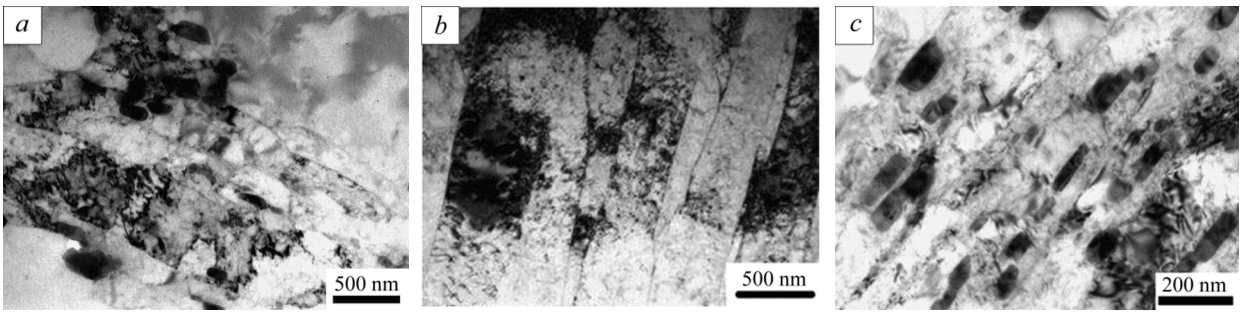

Fig. 1. TEM images showing the structure of steel in the initial hot-rolled state (*a*) and after quenching (*b*) and tempering (*c*).

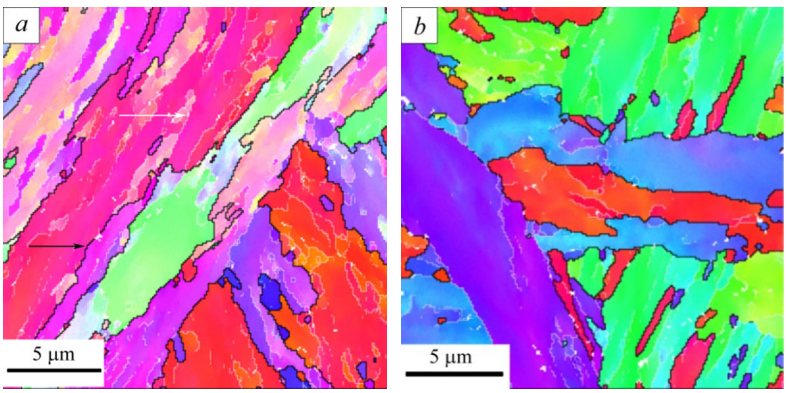

Fig. 2. Inverse pole figure (IPF) maps of the microstructure observed by the electron beam scattered diffraction (EBSD) after quenching (*a*) and tempering (*b*). ▭ LAGB < 15°, ▬ HAGB > 15°.

for 1 h. As a result of quenching, martensitic laths containing high dislocation density were observed (Fig. 1*b*). Tempering led to a more equilibrium microstructure, the distribution of particles throughout the volume occurred more uniformly, and they were located along the boundaries of former lath martensite (Fig. 1*c*).

After quenching, the martensitic structure with an average plate width of 3.4 ± 0.3 μm is observed (Fig. 2*a*). In this case, in comparison with the initial state, the particles of the second phases were not detected. Standard treatment (tempering) led to an increase in the average width of the plates to 5.8 ± 0.6 μm (Fig. 2*b*).

TEM images after cold rolling to 70% reduction (CR70%) demonstrate the formation of a stripe structure with an average lath width of 200 nm and carbides located at the boundaries of laths and blocks (Fig. 3*a*). After rolling to 70% reduction and re-quenching, the formation of equiaxed grains with a size of 2 μm and coarsened carbides are observed (Fig. 3*b*).

EBSD studies of samples after CR50% has demonstrated that the samples have elongated structure with the average plate width of 4.1 μm (Fig. 4*a* and Table 2). The share of high-angle grain boundaries (HAGB) did not exceed 25%, and the share of the coincident site lattice (CSL) boundaries, including twins Σ3 and Σ11, was 1.4%. After CR50% + RQ, the HAGB share increased to 64%, of which the share of the CSL boundaries exceeded 9% (Fig. 4*b* and Table 2). EBSD investigations showed that CR70% results in a HAGB share of 44%. The share of the CSL boundaries was equal to 1.2% (Fig. 4*c* and Table 2). A bimodal structure elongated in the rolling direction with a plate width of 0.5 μm and a length up to 10 μm was formed. A developed subgrain structure was also observed inside the strips. There were chains of smaller and equiaxed grains formed due to the growth of orientations within the original stripes. After CR70% + RQ, the HAGB share did not exceed 34%. The share of the CSL boundaries increased to 6.9% (Fig. 4*d* and Table 2). One can see an equiaxed microstructure with an average grain size of 0.9 μm.

TABLE 2. Microstructure Parameters from the EBSD

Treatment	Grain size, μm	Plate width, μm	HAGB, %	CSL boundaries, %
Tempering	–	5.8 ± 0.4	39 ± 0.3	10.1 ± 0.1
CR50%	–	4.1 ± 0.3	25 ± 0.3	1.4 ± 0.1
CR50% + RQ	2.0 ± 0.3	–	64 ± 0.3	9.1 ± 0.1
CR70%	–	0.6 ± 0.2	44 ± 0.3	1.2 ± 0.1
CR70% + RQ	0.9 ± 0.5	–	34 ± 0.2	6.9 ± 0.1

TABLE 3. Microstructure Parameters from X-ray Diffraction

Treatment	Lattice parameter, A	Dislocation density, 10^{15} m^{-2}	Fraction of carbides, %			
			$Cr_{23}C_6$	Fe_3C	Fe_3W_3C	Total
Tempering	2.87824(8)	1.23	0.82	0.46	0.62	1.9
CR50%	2.87985(8)	2.58	1.21	0.45	0.71	2.37
CR70%	2.88015(9)	3.24	1.42	0.43	0.78	2.63
CR70% + RQ	2.88187(7)	3.05	1.72	0.56	0.89	3.17

TABLE 4. Mechanical Steel Properties after Various Treatments

Treatment	UTS, MPa	δ, %	Impact toughness KCV–40, kJ/m^2
Tempering	900	6.5	25
CR50%	1220	14	200
CR50% + RQ	1380	17	550
CR70%	1250	11	–
CR70% + RQ	1230	15	–

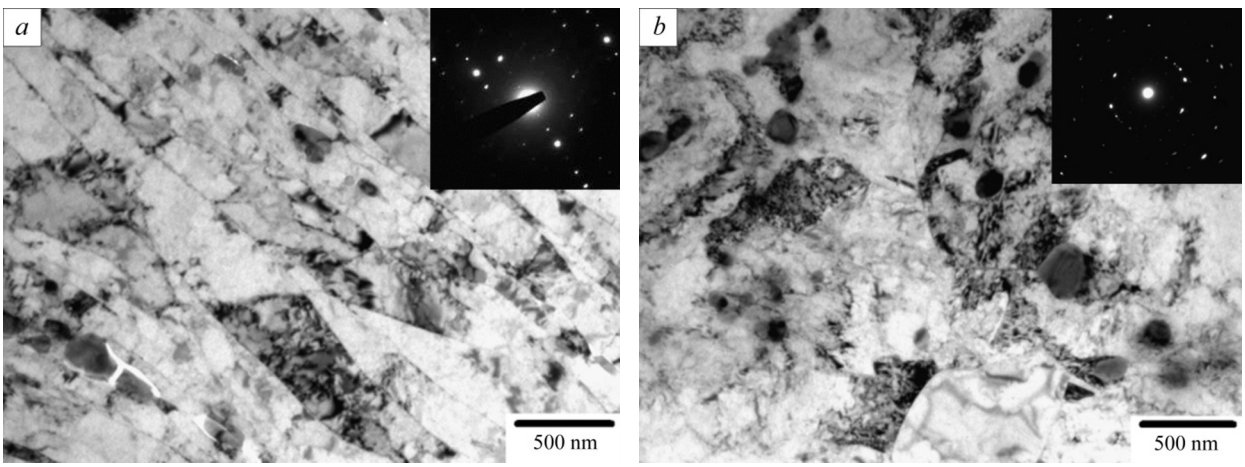

Fig. 3. TEM images of samples after CR70% (*a*) and CR70% + re-quenching (RQ) (*b*).

Figure 5 demonstrates improving the mechanical tensile properties of the 12Cr–2W ferritic/martensitic steel (Table 4). When the thickness reduction reaches 50%, the ultimate tensile strength (UTS) achieves 1220 MPa; a further increase in the thickness reduction to 70% does not lead to a significant increase in the UTS. The use of additional re-quenching (RQ) made it possible to improve the properties. For example, after CR50% + RQ, the UTS increased to 1380 MPa, that is, by more than 50% compared to the samples after standard treatment (tempering), while the ductility was 17% (Table 4). The significant increase in the strength in this case can be explained by both grain refinement and increase in the share of the CSL boundaries after re-quenching (Table 2).

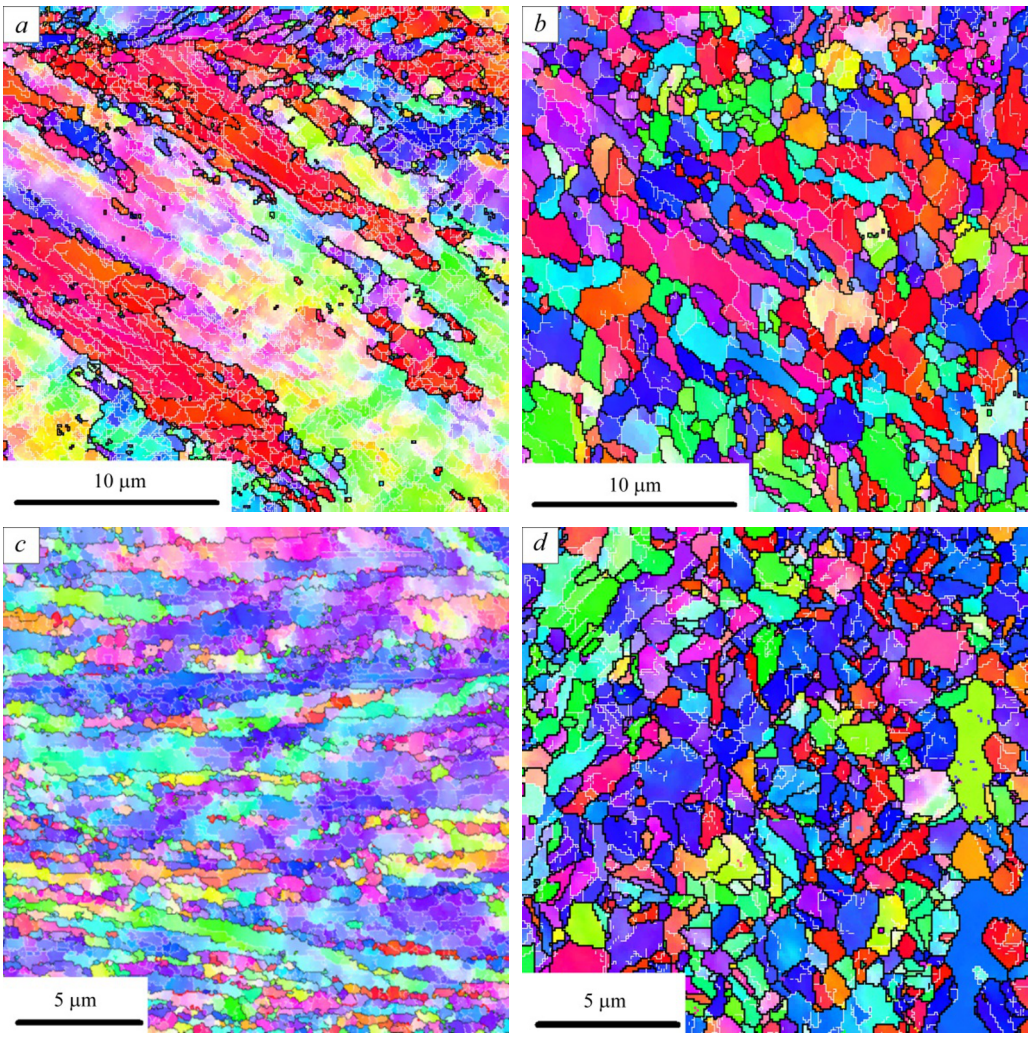

Fig. 4. IPF maps of the steel microstructure after CR50% (*a*), CR50% + RQ (*b*), CR70% (*c*), CR70% + RQ (*d*). The low-angle grain boundaries (LAGB) are marked in white, and the high-angle grain boundaries (HAGB) are marked in black. ▭ LAGB < 15°, ▬ HAGB > 15°.

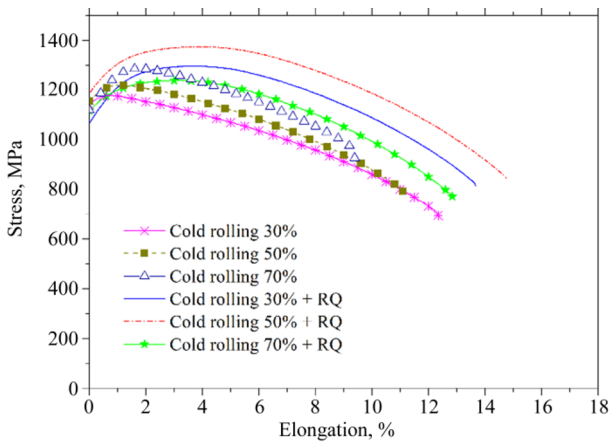

Fig. 5. Stress-strain diagram of the 12Cr–2W ferritic/martensitic steel after various treatments.

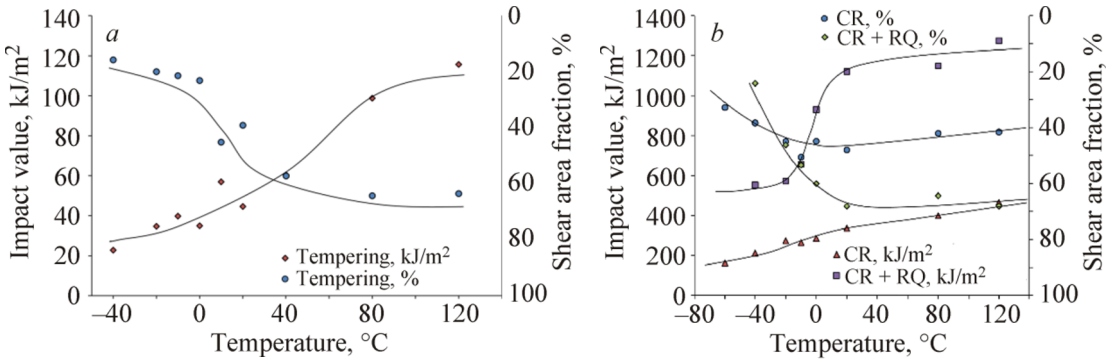

Fig. 6. DBTT after tempering (*a*) and CR50% and CR50% + RQ (*b*).

Figure 6*a* shows the dependences of the impact toughness and ductile fracture fraction for steel after standard treatment (tempering). The DBTT was determined based on achieving 50% of the ductile fracture fraction on the fracture surface. After standard treatment, the DBTT of steel corresponds to +20°C. Impact toughness KCV at temperatures of –40, 20, and 120°C corresponded to 25, 45, and 120 kJ/m^2, respectively. The results of studying the impact toughness of steel after CR50% are shown in Fig. 6*b*. After CR50%, the DBTT corresponds to –20°C. The impact toughness KCV at temperatures of –40, 20, and 120°C was equal to 200, 250, and 460 kJ/m^2, respectively. After CR50% + RQ, the DBTT also corresponded to –20°C (Fig. 6*b*). The impact toughness was by several times higher compared to that of the samples subjected to standard treatment or CR50% + RQ. For example, at temperatures of –40, –10, and 120°C, it was equal to 550, 650, and 1200 kJ/m^2, respectively. It is worth noting that the use of the additional re-quenching led to a slight (by 10°) decrease in the DBTT from –10 to –20°C. However, at the same time, the impact toughness increased almost 3 times over the entire temperature range. The most critical KCV at –40°C increases from 160 to 550 kJ/m^2.

DISCUSSION

Generally, steels become brittle (have low ductility and low toughness) after grain refinement when they have enhanced strength, and they become ductile (have high ductility and high toughness) at low strength after grain coarsening [4]. At the same time, it has been demonstrated recently the possibility to increase the impact toughness in the ultra-fine grained (UFG) metallic materials by grain refinemrnt and additional heat treatment [9]. Results presented in Table 4 and in Fig. 5 have demonstrated simultaneously the enhanced strength in the ferritic/martensitic steel processed by cold rolling to 50% reduction and additional re-quenching (CR50% + RQ) compared to the standard treatment (tempering) and CR70% + QR. The reason for such unusual mechanical behavior in the CR50% + RQ samples is apparently caused by structural changes at this treatment. Despite the finer grain size in the CR70% + QR, the fraction of the HAGB (64%) and the CSL boundaries (9.1%) is higher in CR50% + RQ (Table 2). Modeling by the viscoplastic self-consistent (VPSC) model [10] have indicated that at the initial stages of rolling, the gliding activity of dislocations along the <111> {110} slip systems is enhanced, whereas in the <111> {123} systems, it is suppressed. The activity of twinning in the <111> {112} systems is also more suppressing (to 70% compared to 50% reduction) [3].

The difference (twice) between the grain sizes of the samples subjected to CR50% and CR50% + QR (Fig. 4) is insufficient to explain the increase of the toughness by several times (Fig. 6*b*). At the same time, the samples after CR50% + RQ have more equiaxed grain structure and the increased share of the CSL boundaries equal to 9.1% compared to a share of 1.4% in the samples subjected to CR50% (Table 2). It is well known that special cases of the CSL boundaries are twins capable to hinder the dislocation gliding near the tip of the crack propagation [11]. Therefore, the unusual increase in the toughness in the high-strength ferritic/martensitic steel after CR50% + RQ compared to the CR50% samples can be explained by both the grain refinement and increased share of the CSL boundaries after additional re-quenching.

The samples subjected to CR50% also demonstrated the increased toughness and ductility compared to the standard treatment (tempering) (Table 4). In this case, a slight decrease in the plate width down to 4.1 μm (CR50%) from 5.8 μm (tempering) is insufficient to increase significantly (be several times) the toughness and ductility (Table 4). The increase in the volume fraction of carbides in the CR50% samples in comparison with tempering (Table 3) leads to additional obstacles for the dislocation gliding near the tip of the crack propagation [12, 13]. On the other hand, the obvious metallographic texture and line arrangement of carbides determine the dependences of the mechanical properties on the sample orientation relative to the direction and plane of rolling [14, 15]. Thus, the enhanced strength and toughness in the ferritic/martensitic steel processed by CR50% + RQ can be explained by the combination of various strengthening mechanisms including grain refinement, dispersion hardening, and increased share of CSL boundaries, because the propagating cracks can be trapped by the corresponding defects of the crystal lattice, for example, the grain boundaries, carbides, and CSL boundaries [16–18].

CONCLUSIONS

1. Application of cold rolling to 50% reduction and additional re-quenching (CR50% + RQ) to the 12Cr–2W ferritic/martensitic steel has led to the equiaxed grain structure with a grain size of 2 μm containing both numerous carbides with fraction of 2.37 and CSL boundaries with a share of 9.1%.

2. The CR50% + RQ samples demonstrated unique combination of the enhanced strength equal to 1380 MPa, ductility of 17%, and high toughness compared to the samples subjected to standard treatment (tempering). The ductile-brittle transition temperature decreased to –20°C after CR50% + RQ.

3. The achievement of the enhanced strength and high toughness in the CR50%+ RQ samples can be explained by the combination of various strengthening mechanisms, including grain refinement, dispersion hardening, and increased share of the CSL boundaries.

COMPLIANCE WITH ETHICAL STANDARDS

Author contributions

A.V.G., A.A.F., R.K.I., N.A.K., and M.A.N. contributed to the design and implementation of the research, to the analysis of the results, and to the writing of the manuscript. All authors have read and agreed to the published version of the manuscript.

Conflicts of interest

The authors declare that they have no known competing financial interests or personal relationships that could have appeared to influence the work reported in this paper.

Funding

This work was supported by the Russian Science Foundation (Project No. 22-19-00445).

Financial interests

The authors have no relevant financial or non-financial interests to disclose.

Institutional review board statement

Applicable.

Acknowledgments

We are grateful to the Center of Collaborative Access "Nanotech" of Ufa University of Science and Technology for supplying the equipment for structural studies and mechanical tests.

REFERENCES

1. M. Song, Y. D. Wu, D. C. X. M. Wang, *et al*., Acta Mater., **74**, 285–295 (2014); https://doi.org/10.1016/j.actamat.2014.04.034.
2. R. K. Islamgaliev, M. A. Nikitina, A. V. Ganeev, *et al*., Mater. Sci. Eng. A, **744**, 163–170 (2019); https://doi.org/10.1016/j.msea.2018.11.141.
3. V. D. Sitdikov, R. K. Islamgaliev, G. F. Sitdikova, *et al*., J. Mater. Sci. Perform., **31** (3), 1971–1980 (2022); https://doi.org/10.1007/s11665-021-06357-0.
4. T. Inoue and R. Ueji, Mater. Sci. Eng. A, **786**, 139415 (2020); https://doi.org/10.1016/j.msea.2020.139415.
5. O. Saray, G. Purcek, I. Karaman, and H. J. Maier., Metall. Mater. Trans., **43A**, 4320–4330 (2012); https:/doi.org/10.1007/s11661-012-1238-x.
6. V. D. Sitdikov, M. Yu. Murashkin, and R. Z. Valiev, J. Mater. Eng. Perform., **26**, 4732–4737 (2017); https://doi.org/10.1007/s11665-017-2915-0.
7. H. M. Rietveld, J. Appl. Crystallogr., **2**, 65–71 (1969); https://doi.org/10.1107/S0021889869006558.
8. F. Abe, Sci. Technol. Adv. Mater., **9**, 012002 (2008); https://doi.org/10.1088/1468-6996/9/1/013002.
9. I. M. Safarov, A. V. Korznikov, R. M. Galeyev, *et al*., Lett. Mater., **6**, No. 2, 126–131 (2016).
10. R. A. Lebensohn and C. N. Tome. Mater. Sci. Eng. A, **175**, 71–82 (1994); https://doi.org/10.1016/0921-5093(94)91047-2.
11. H. Luo, X. Wang, Z. Liu, *et al*., J. Mater. Sci. Technol., **51**, 130–136 (2020); https://doi.org/10.1016/j.jmst.2020.04.001.
12. V. Dudko, J. Borisova, and R. Kaibyshev, Acta Phys. Pol. A, 134, 649–652 (2018); https://doi.org/10.12693/APhysPolA.134.649.
13. M. V. Odnobokova, A. Yu. Kipelova, A. N. Belyakov, *et al*., Phys. Met. Metallogr., **117**, 390–398 (2016); https://doi.org/10.1134/S0031918X16040098.
14. Y. Kimura, Metall. Mater. Trans. A, **44**, 560–576 (2013); https://doi.org/10.1007/s11661-012-1391-2.
15. N. Polekhina, V. Linnik, I. Litovchenko, *et al*., Russ. Phys. J., **66**, 404–409 (2023); https://doi.org/10.3390/met12111928.
16. Y. J. Zhao, Y. M. Su, M. Liu, *et al*., Strength Mater., **51**, 291–299 (2019); https://doi.org/10.1007/s11223-019-00075-8.
17. J. Reiser and A. Hartmaier, Sci. Rep., **10** (1), (2020); https://doi.org/10.1038/s41598-020-59405-5.
18. M. Huang, C. Wang, X. Zhu, *et al*., Metall. Mater. Trans., **53A**, 1921–1927 (2022).